Geomechanics and Engineering, *Vol. 42, No. 6 (2025) 453-462*
https://doi.org/10.12989/gae.2025.42.6.453

Long-term response of granular materials subjected to repetitive mechanical loads: Engineering implications

Wonjun Cha[1], Sang Yeob Kim[2], Young Chan Kim[3] and Junghee Park*[3]

[1]*Department of Civil Engineering, University of Birmingham, Edgbaston, Birmingham, B15 2TT, UK*
[2]*Department of Fire and Disaster Prevention, Konkuk University, 268, Chungwon-daero, Chungju, 27478, Republic of Korea*
[3]*Department of Civil and Environmental Engineering, Incheon National University, 119 Academy-ro, Yeonsu-gu, Incheon 22012, Republic of Korea*

(*Received May 21, 2025, Revised September 1, 2025, Accepted September 11, 2025*)

Abstract. This study investigates the long-term response of granular materials subjected to repetitive mechanical loads through integrated experimental and numerical approaches. Repetitive Ko-loading tests, triaxial tests, and simple shear tests reveal two critical asymptotic states governing system behavior: (1) a terminal void ratio controlling volumetric stabilization, and (2) stress-obliquity-dependent shear modes transitioning between shakedown and ratcheting. Results demonstrate that repetitive loading alters the coefficient of earth pressure through fabric evolution, quantified via shear wave velocity-stress relationships. Granular degradation analyses show particle abrasion dominates at low-stress/high-cycle conditions, while fines content critically influences deformation response through threshold fines fractions. A new dimensionless shear stress ratio successfully predicts long-term shear response between shakedown and ratcheting. Hybrid numerical modeling combining conventional constitutive model with empirical strain accumulation reduces computational errors and enhance convergency to conventional methods for high-cycle simulations.

Keywords: energy geosystems; ratcheting; repetitive mechanical loads; shakedown; terminal void ratio

1. Introduction

Geosystems and granular materials often experience repetitive loads. Associated examples involve carbon free energy-related geosystems such as pumped hydro storage, compressed air energy storage, geothermal heat pump and energy storage and stored energy in waste. Repetitive load-induced stress paths imposed on geosystems are complex and vary with the type of geo-structures, loading direction, periodicity and boundary conditions (Pasten and Santamarina 2011).

In particular, modes of repetitive loads under different boundary conditions play a critical role in the determination of gradual deterioration of geo-material properties rather than monotonic failure. The long-term performance of geo-storage systems, serviceability, and safety. All kinds of repetitive loads gain relevance in the long-term performance and engineering design of geo-structures and energy-related geosystems. Indeed, the long-term performance of energy geosystems subjected to repetitive loads requires test protocols and devices, suitable models and algorithms in numerical simulation.

This study identifies modes of repetitive mechanical loads under different imposed boundary conditions. Next, we attempt to anticipate the asymptotic volumetric and shear trends using a physics-inspired and data-centered approach. Accumulation models and an extensive dataset available from published literature allow for simple and robust first-order estimates of the maximum settlement or shear modes a geosystem may experience during repetitive loading. Finally, we explore the numerical simulations and close-form estimates to assess emergent phenomena and coupled processes that contribute to the long-term implementation of energy geo- systems when subjected to repetitive mechanical loads. The modeling framework developed in this study provides clear engineering outcomes: practical tools for settlement estimation and hybrid computational strategies for high-cycle simulation challenges.

2. Modes of repetitive mechanical loads

2.1 K_o-Loading (Zero Lateral Strain Conditions)

Laboratory repetitive load studies using the oedometric system assume the zero-lateral strain conditions and facilitate a first-order estimate of the maximum plastic deformation a sediment may experience beneath a foundation when subjected to an infinite loading cycles (see relevant examples in Chong and Santamarina 2016, Park and Santamarina 2019). Figure 1 shows a typical repetitive load-deformation response of soils subjected to Ko-loading cycles.

The purpose of the K_o-loading experiments was to isolate the purely volumetric response of granular materials

*Corresponding author, Ph.D.
E-mail: junghee.park@inu.ac.kr

ISSN: 2005-307X (Print), 2092-6219 (Online)

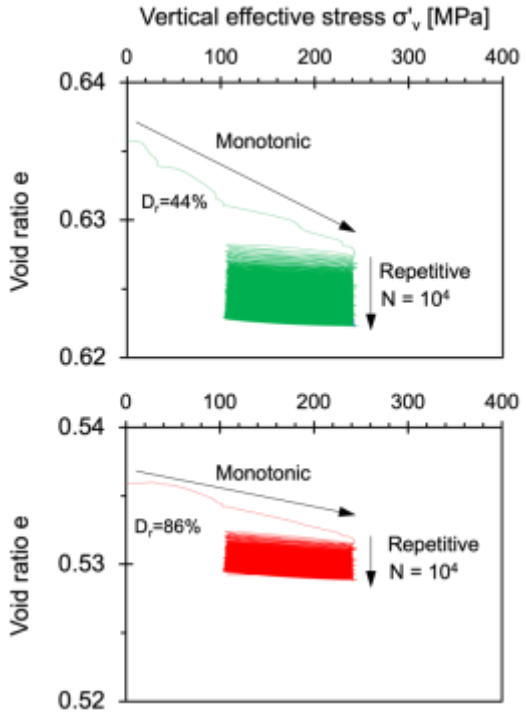

Fig. 1 The change in void ratio during the static–repetitive–static loading history. Test conditions: σ_o= 105 kPa, stress amplitude ratio $\Delta\sigma/\sigma_o$ = 1.3 from 105-to-243 kPa (modified from Park and Santamarina 2019)

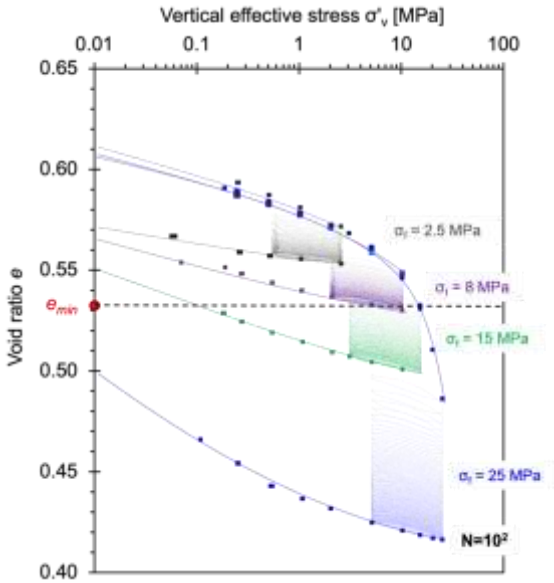

Fig. 2 The change in void ratio during the static–repetitive–static loading history followed by the static unloading sequence: High stress amplitude repetitive loading tests - Void ratio evolution (N= 100 cycles - KAUST 20/30 sand). For reference, the minimum void ratio is e_{min}= 0.533 (Modified from Park and Santamarina 2023)

under repetitive loading. These tests allowed identification of the terminal void ratio e_T, which defines the maximum long-term settlement, and enabled us to monitor the dynamic evolution of the earth pressure coefficient K_o via

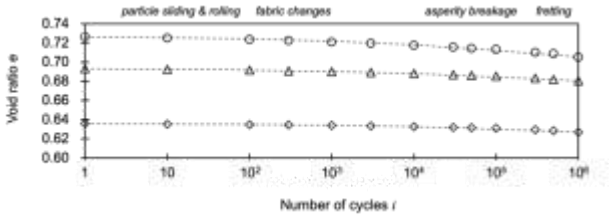

Fig. 3 Low-stress amplitude repetitive loading tests - Void ratio evolution (N= 10^6 cycles - KAUST 20/30 sand). The three tests start at different void ratios e_o: initial vertical stress σ_o= 67 kPa, and vertical stress cyclic amplitude $\Delta\sigma$= 100 kPa (from σ = 67-to-167 kPa). (Modified from Park and Santamarina 2023)

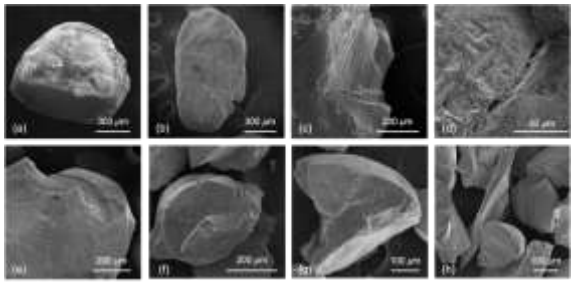

Fig. 4 Scanning Electron Microscope SEM images: (a) Abrasion and fretting on the particle surface. (b) Asperity breakage. (c) Planar surface from tensile splitting. (d) Micro fracture. (e) V-shaped pits. (f) Clean fracture surface. (g) Conchoidal fracture. (h) Preferential splitting of finer particles along cleavage planes. Note: blade-shaped particles prevail among the finer produced particles

shear wave velocity measurements. This section reports detailed reviews about processes and phenomena under repetitive Ko-loading conditions.

Granular degradation. Repetitive mechanical loads lead to granular degradation that influences the long-term performance of engineered geosystems. Fines produced during granular degradation increase the difficulties in predicting engineering properties such as shear strength, compressibility, and hydraulic conductivity. Relevant phenomena include the decrease in pore size, increase in specific surface, and the consequence of fines migration, entrapment, bridging, and clogging (Feda 2002, Sadrekarimi and Olson 2010, Hafez *et al.* 2021). Fines produced during repetitive loading also trigger the undrained failure of railway ballast (Indraratna and Redana 1997).

Figs. 2 and 3 shows the volume change during the repetitive high stress loading cycles and one million loading cycles which involve both fabric change and granular degradation.

The strain level determines the underlying particle-scale deformation mechanisms. Elastic deformations at grain contacts prevail and the fabric remains constant as the strain level imposed on soils is smaller than the elastic threshold strain. On the other hand, there are minimal fabric changes until the volumetric threshold strain. However, it remains

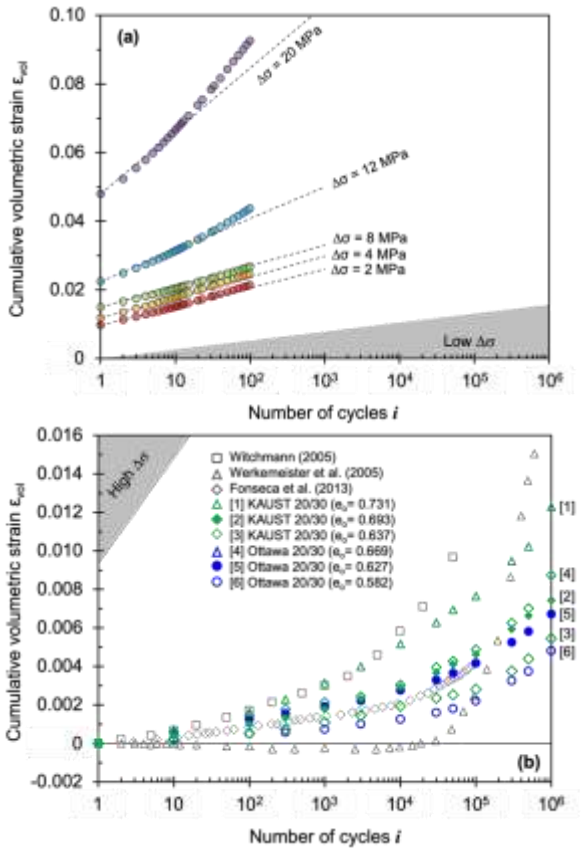

Fig. 5 Cumulative volumetric strain ε_{vol} with number of cycles. (a) N= 10^2 high-stress cycles (KAUST 20/30 sand). (b) N= 10^6 low-stress cycles (KAUST 20/30 sand and complementary data gathered with Ottawa 20/30 sand). Note differences in strain scale. (Modified from Park and Santamarina 2023)

unclear whether the elastic threshold strain obtained under quasi-static loading conditions also applies to the soil response in repetitive loading. Granular degradation mechanisms depend on the final stress level and the number of cycles (i.e., Both ends of the Wöhler's curve). For example, particle crushing or splitting should be dominant for even few numbers of high-stress cycles while surface abrasion and fretting and asperity breakage may prevail at large number of low-stress cycles (Fig. 4). Data show "tipping points" in the load-deformation response at a large number of cycles, despite relatively low levels of stress amplitudes (Fig. 5 - see data in Werkmeister *et al.* 2005). The non-linear response in the plastic strain ε_{pl} versus number of cycles challenges the prediction of permanent strain accumulation.

Coarse-fine mixtures. The presence of fines in soil mixtures plays a critical role in long-term mechanical response of sand-fines mixtures in plastic strain accumulation when subjected to repetitive loading under zero-lateral strain conditions. In all cases, the void ratio evolution of sand-fines mixtures with different fines fractions exhibits asymptotic terminal void ratio e_T as the number of cycles increases (Fig. 6). Previous studies recognized the importance of fines and used the volumetric-

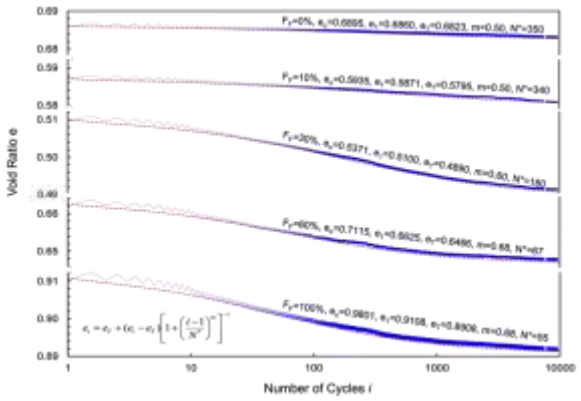

Fig. 6 Void ratio evolution for sand-fines mixtures with number of cycles *i*. Test conditions: σ_o= 67 kPa, stress amplitude ratio $\Delta\sigma/\sigma_o$= 1.50 (from 67-to-167 kPa) (Modified from Kim *et al*. 2021)

gravimetric analysis to define the threshold fines fraction F_{th} (Park and Santamarina 2017). The low and high threshold fines fractions adequately bound the fines-controlled, the coarse-controlled, and transitional zone in sand-fines mixtures. Indeed, fines separate coarse grains apart or fines tends to occupy the pores between the coarse grains in the transitional mixtures. The terminal void ratio e_T, asymptotic contraction $\Delta e=e_o-e_T$, and volumetric strain data trends capture the transition of the sand-to-fines controlled repetitive load-deformation behavior.

Resilient modulus. A key objective of the mechanistic pavement design aims to allow resilient deformations only in the pavements when subjected to traffic-induced repetitive loadings. From the particle scale point of view, resilient strains mainly result from deformations of the individual grains (Werkmeister *et al*. 2005; Park and Santamarina 2019, Qiu *et al*. 2025). For long-term mechanical performance of pavements, unbound granular layers UGL should be able to resist plastic deformation above a certain tolerable level. In this context, pavement design adopts the resilient modulus $M_r = \sigma_d/\varepsilon_r$ to define the stiffness of pavement layers where σ_d corresponds to the applied vertical stress and ε_r to the recoverable axial strain in a cyclic triaxial test (Hicks and Monismith 1971).

Previous laboratory test protocols provide the resilient modulus of granular bases (Tutumluer and Seyhan 1999, see detailed test procedure for resilient modulus in NCHRP 2004). These tests attempt to reproduce soil compaction and loading history associated with field conditions. However, previous methods do not properly simulate roller compaction, and the stress conditions used in resilient modulus determination and they cannot reflect the complexity of the loading history and stress field granular base may experience under working conditions (Kim and Tutumluer 2005). Furthermore, the inherent stress-induced anisotropy of the granular base stiffness plays a critical role in pavement response; yet, its consideration remains overlooked in most tests (Al-Qadi *et al*. 2010).

Alternatively, most numerical simulations use a secant stiffness formulation to capture the stiffness of granular

layers as a function of the state of stress during traffic loading (Hicks and Monismith 1971, Brown 1996). However, one may wonder whether the secant formulation handle the apparent incremental material response and any arbitrary stress path. In this context, a recently-proposed new tangent model appears to properly capture the stress-dependent resilient stiffness of granular bases (Papadopoulos and Santamarina 2016). This new formulation uses a modulus reduction rule, captures stress-hardening, shear-softening and stress-induced anisotropy, and anticipates the load-deformation response of unbound granular bases from small-to-intermediate strain levels. In both laboratory tests and numerical simulation, the stress-induced anisotropy appears to be critical in the determination of the granular base stiffness.

In the field, there are several conventional techniques for the in-situ stiffness measurement of unbound granular layers such as falling weight deflectometer FWD, light weight deflectometer LWD and the seismic pavement analyzer SPA (Fleming *et al.* 2007). In general, conventional in-situ stiffness measurement methods still contain limitations such as unknown state of stress in pavements, anisotropic stiffness of unbound granular layers, inverse problem solving for the interpretation of boundary measurements at the pavement surface, and inversion-related measurement errors and uncertainty of inferred outcome (Papadopoulos *et al.* 2016). In this context, the direct measurement of in-situ small-strain stiffness of unbound granular materials using seismic techniques under controlled surface loading conditions seems to be a simple but robust approach. Recent investigations have reported the strong mechanistic correlation between small strain stiffness estimated using wave propagation and resilient modulus of granular bases (Williams and Nazarian 2007, Schuettpelz *et al.* 2010).

Small strain stiffness. The shear wave velocity is a power function of the vertical σ′v and horizontal σ′h effective stresses where the coefficient of earth pressure at rest Ko= σ′h/σ′v (vertical propagation, horizontally polarized - Yu and Richard 1984, Santamarina *et al.* 2001)

$$V_S = \alpha\left(\frac{\sigma_v^{'}+\sigma_h^{'}}{2\,kPa}\right)^{\beta} = \alpha\left(\frac{\sigma_v^{'}}{1kPa}\right)^{\beta}\left(\frac{1+K_o}{2}\right)^{\beta} \quad (1)$$

where the α-factor indicates the shear wave velocity at effective stress $(\sigma'_v + \sigma'_h)/2 = \sigma'_{mean}$ = 1 kPa, and the β-exponent reflects the sensitivity of the shear wave velocity to the effective stress changes. The shear wave velocity-stress relation captures both contact behavior during low-perturbation wave propagation and fabric changes related with effective stress variations (Cha *et al*. 2014).

Low-perturbation wave propagation built on the shear wave velocity-stress relation successfully captures both contact behavior and fabric changes related with effective stress variations. The shear wave velocity V_S and maximum shear stiffness G_{max} at small strain regime reflect the assessment of state at a quasi-constant fabric. Small strain stiffness is a function of coordination number CN and contact flatness that reflects contact stiffness through the fabric at a given stress state.

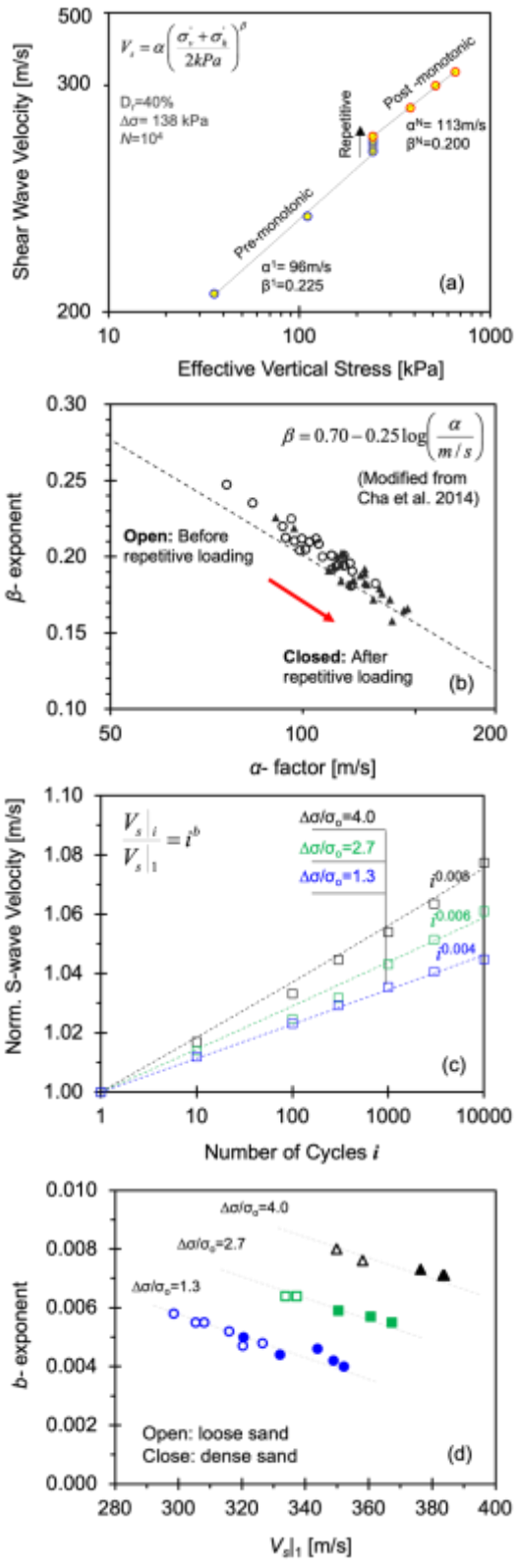

Fig. 7 The evolution of shear wave velocity during static and repetitive loading stages: (a) shear wave velocity plotted against stress, (b) the α factor and β exponent before and after repetitive mechanical loading, (c) normalised shear wave velocity plotted against number of cycles and (d) the d exponent plotted against shear wave velocity at the beginning of repetitive loading, $Vs|_1$ (Modified from Park and Santamarina 2019)

Fig. 7 summarizes the changes in shear wave velocity measured during the (1) static, (2) repetitive, and (3) static loading stages for loose and dense sands. Fig. 7(b) presents the α-factors and β-exponents computed by fitting Equation 1 to the static load stages before and after repetitive loading for all tests. The data trend is consistent with the relationship between α and β values reported by Cha *et al.* (2014). Overall, the sand becomes stiffer (i.e., lower C_c), the α-factor increases, the β-exponent decreases and the soil fabric becomes less sensitive to stress changes after repetitive loading

$$\frac{V_s|_i}{V_s|_1} = i^b \tag{2}$$

The b-exponent tends to decrease with higher shear wave velocity for the first cycle $V_s|_1$ (Fig. 7(d)). The increase rate of small-strain shear stiffness during repetitive loading becomes more pronounced in looser sands subjected to high stress cycles where more significant fabric changes take place.

The P-wave velocity V_P corresponds to the maximum constrained modulus $M_{max} = \rho \cdot V_P^2$ through the bulk density ρ and S-wave velocity V_S to maximum shear modulus $G_{max} = \rho \cdot V_S^2$. Once again, recent mechanistic pavement studies confirm that there exists the strong correlation between small strain stiffness inferred using elastic wave velocity and resilient modulus of granular bases (Williams and Nazarian 2007, Schuettpelz *et al.* 2010). The stiffness ratio between the resilient modulus E_r and the maximum stiffness E_{max} computed from elastic wave velocity is in the range of $E_r/E_{max} \approx$0.4-to-0.8 (Davich *et al.* 2004, Schuettpelz *et al.* 2010). Similar concepts apply to all foundation systems subjected to repetitive mechanical loads. For example, the resilient constrained modulus M_r measured in 1-D oedometer tests is the ratio between the stress amplitude $\Delta\sigma$ and the peak-to-peak strain ε_{pp} in the i-th cycle (i.e., $M_r = \Delta\sigma/\varepsilon_{pp}$). Then, the small strain shear modulus $G_{max} = \rho \cdot V_s^2$ is a function of density ρ and shear wave velocity V_S. Figure 8a shows the evolution of the stiffness ratio M_r/G_{max} versus the number of cycles for N=10^2 high-stress and N=10^6 low-stress tests; for comparison, Fig. 8(b) presents previously published data. The stiffness ratio M_r/G_{max} ranges between $0.85 \le M_r/G_{max} \le 2.25$, increases with the number of cycles, and higher ratios correspond to higher peak cyclic stress σ_{peak} and lower densities.

The peak-to-peak strain level is $\varepsilon_{pp} \sim$ 3-to-8 $\times 10^{-3}$ in high-stress cycles, $\varepsilon_{pp} \sim$ 2-to-4 $\times 10^{-4}$ in low-stress-stress cycle tests, and about $\varepsilon_{pp} \sim 10^{-8}$ in wave propagation measurements. Clearly, the resilient constrained modulus M_r and the small-strain shear modulus G_{max} are in the different strain levels and involve different values of Poisson's ratio. Therefore, the relationship between E_r/E_{max} and M_r/G_{max} requires a small-strain Poisson value $\nu_o = 0.10$ to relate E_{max} to G_{max} and an intermediate-strain Poisson value $\nu_r = 0.25$ to link E_r and M_r

$$\frac{M_r}{G_{max}} = \frac{\dfrac{E_r(1-\nu_r)}{(1+\nu_r)(1-2\nu_r)}}{\dfrac{E_{max}}{2(1+\nu_o)}} = \frac{E_r}{E_{max}} \cdot \frac{2(1-\nu_r)(1+\nu_o)}{(1+\nu_r)(1-2\nu_r)} \tag{3}$$

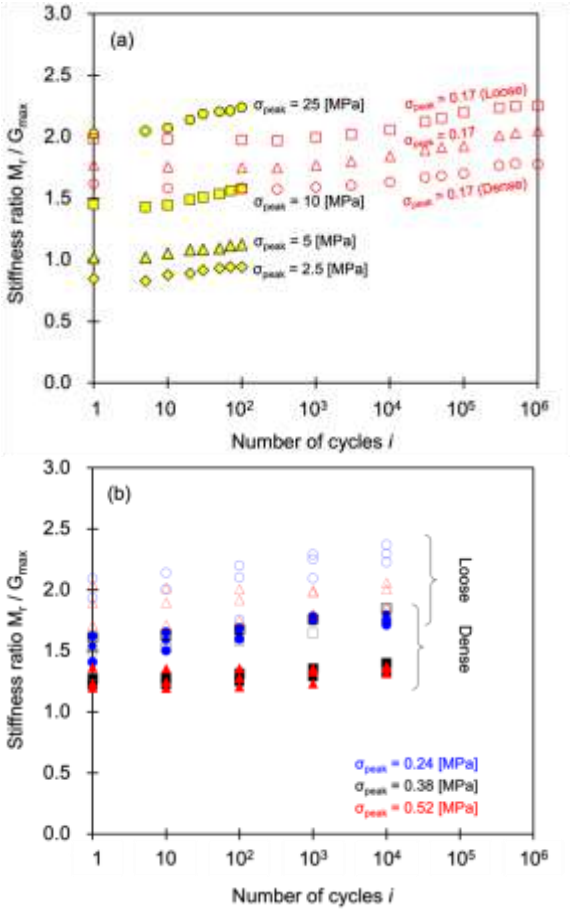

Fig. 8 Stiffness ratio M_r/G_{max} versus number of cycles. The mid-strain resilient constrained modulus M_r and the maximum shear modulus G_{max} measured small strain shear wave propagation. (a) 10^2 high-stress and 10^6 low-stress cycles (b) 10^4 intermediate stress cycles (Modified from Park and Santamarina 2019)

For the selected Poisson's ratios ν_o= 0.10 and ν_r= 0.25, the ratio $(M_r/G_{max})/(E_r/E_{max}) \approx 2.6$ agrees with the data. This physics-based and data-centered analysis demonstrates that the mechanistic approach is convenient for engineering implications.

K_o evolution. The coefficient of earth pressure $K_o = \sigma'_h/\sigma'_v$ at rest is the ratio between vertical and horizontal effective stresses. This ratio varies with the initial soil density, over consolidation ratio OCR, and changes in the in-situ stress state under zero-lateral strain conditions (Mayne and Kulhawy 1982). The coefficient of earth pressure K_o at rest tends to decreases with higher initial void ratio (Daramola 1980). Repetitive mechanical loads also alter the coefficient of earth pressure K_o. Previous examination shows that the horizontal stress during a constant stress amplitude cycle decreases as the number of cycles increases for high OCR specimens (Sawicki and Swidzinski 1995). The evolution of K_o follows the logarithmic trend as a function of cycle number.

The shear wave velocity gathered during the repetitive loading with the modified oedometer cell allow us

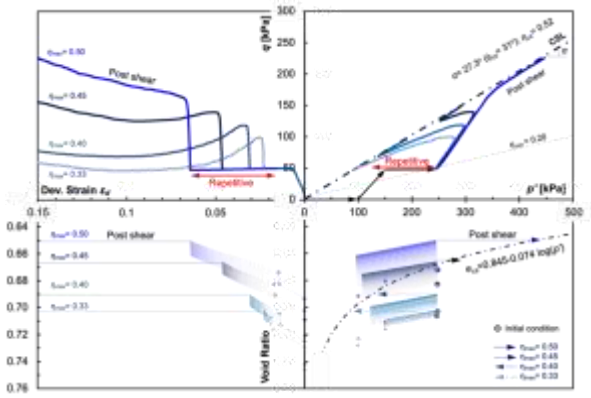

Fig. 9 Maximum stress obliquity: Loose and medium dense sands subjected to repetitive fluid pressure cycles to different maximum stress obliquities η_{max}. In all four specimens, the pressure cycles begin at p'=250 kPa and η_{min}=0.20. Tests end with undrained axial compression from the same initial stress condition at η_{min}=0.20. Notation: $p'=(\sigma_1'+\sigma_3')/2$, $q=(\sigma_1'-\sigma_3')/2$, $\phi_{cs}=\sin^{-1}(\tan\alpha)$, and stress obliquity $\eta=q/p'$ (Modified from Park *et al.* 2020)

to predict the evolution of the coefficient of earth pressure K_o during repetitive loading (Figure 7a). From Eq. (1)

$$\frac{V_s|_N}{V_s|_1}=\frac{\alpha|_N}{\alpha|_1}\frac{\left(\frac{\sigma_z'|_N}{1kPa}\right)^{\beta|_N}}{\left(\frac{\sigma_z'|_1}{1kPa}\right)^{\beta|_1}}\frac{\left(\frac{1+K_o|_N}{2}\right)^{\beta|_N}}{\left(\frac{1+K_o|_1}{2}\right)^{\beta|_1}} \tag{4}$$

where the subscript 1 corresponds to cycle number i = 1 and N to the final loading cycles. Then, the coefficient of earth pressure K_o after N_{th} cycles $K_o|_N$ is

$$K_o|_N=\frac{\sigma_h'}{\sigma_v'}=2\left[\frac{V_s|_N}{V_s|_1}\frac{\alpha|_1}{\alpha|_N}\sigma_v'^{(\beta|_1-\beta|_N)}\left(\frac{1+K_o|_1}{2}\right)^{\beta|_1}\right]^{\frac{1}{\beta|_N}}-1 \tag{5}$$

Assuming a nominal initial value $K_o|_1$= 0.42, the α and β values fitted before and after repetitive loading allow us to anticipate a stress ratio $K_o|_N \approx 0.48 \pm 0.02$ immediately after repetitive loading with stress amplitude ratio $\Delta\sigma/\sigma_o$=1.3 (see data in Park and Santamarina 2019 and similar trend in Sawicki and Swidzinski 1995). Hence, indirect shear wave velocity measurements suggest a gradual increase in horizontal stress during repetitive loading under zero lateral strain conditions.

2.2 Repetitive triaxial loading

The drained repetitive triaxial test controls the vertical stress amplitude and confinement to reproduce complex stress and strain paths and measurements provide a complete load-deformation response in p'-q-e-ε_d spaces. Fig. 9 shows the long-term response of loose and medium dense sand subjected to repetitive fluid pressure cycles under triaxial conditions (Park and Santamarina 2020). Vertical strain accumulation depends on the initial void ratio e_o, the initial confinement p'_o, and the maximum stress

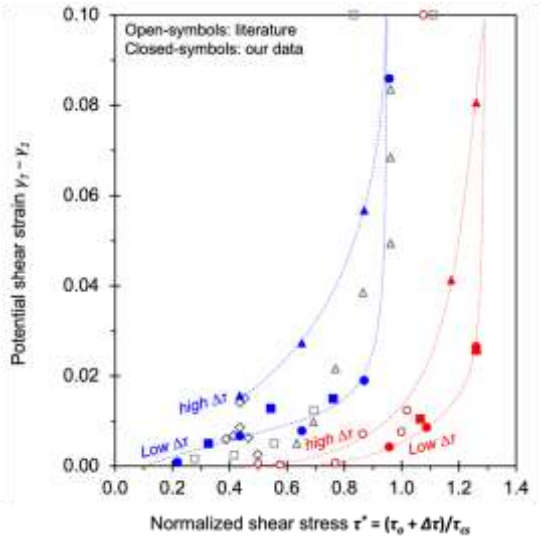

Fig. 10 Shakedown and ratcheting trends in terms of density and normalized shear stress $\tau^*=(\tau_o+\Delta\tau)/\tau_{ult}$. Potential change in shear strain $\Delta\gamma=\gamma_T-\gamma_1$. Blue colors: "contractive" specimens; red colors: "dilative" specimens. Note: Initial shear stress τ_o and shear stress amplitude $\Delta\tau$ are absolute values. Filled symbols: data measured in this study. Open symbols: triaxial data from the literature (Modified after Cha *et al.* 2023)

obliquity η_{max}. The change in void ratio also becomes pronounced as the maximum stress obliquity η_{max} increases. Further observations confirm that higher deviatoric stress amplitude Δq and average stress obliquity η_{avg} develop the larger shear and volumetric strain accumulation for the contractive specimens (Werkmeister *et al.* 2005, Wichtmann *et al.* 2005, Wu *et al*. 2017).

2.3 Repetitive simple shear

Repetitive simple shear tests are suitable to emulate the load boundary conditions of soil elements next to the pile foundations and beneath of pavement (Anderson 2009). These geosystems often experience mechanical loading cycles and soils adjacent to structures exhibit shear and volumetric strain accumulations. Previous shakedown studies establish criteria to predict the shakedown-dominant zone in a p'-q quadrant (Lekarp and Dawson 1998, Werkmeister *et al*. 2005). Yet, there is a limitation that dilatancy and stress history is not considered. In this context, new enhanced engineering chart (Fig. 10) predict the shear mode under repetitive shear loading with the dimensionless shear stress ratio $\tau^*=(\tau_o+\Delta\tau)/\tau_{ult}$ to considers initial shear stress τ_o, shear stress amplitude $\Delta\tau$, the ultimate strength τ_{ult} measured in monotonic shear at a constant vertical stress σ_v, and initial packing density (Cha *et al.* 2023).

3. Modeling and engineering

3.1 Databases - normalization

The heterogeneous nature of granular materials reported

in literature, including variations in gradation compositions and material types, necessitates a robust normalization framework to ensure data credibility and meaningful cross-study comparisons. This study addresses these concerns through a systematic dual normalization approach.

(1) Packing State Normalization. Initial relative density D_o normalizes the packing state, enabling comparison of materials with different void ratio ranges (e_{max}-e_{min}) and density characteristics.

(2) Stress State Normalization The dimensionless shear stress ratio $\tau^*=(\tau_o+\Delta\tau)/\tau_{ult}$ normalizes applied stresses by each material's ultimate strength, effectively removing material-specific strength variations from the analysis. This enables identification of universal behavioral patterns independent of specific material properties.

The strain accumulation model captures the asymptotic terminal void ratio e_T. The ratio between the asymptotic contraction $\Delta e = e_o - e_T$ and the attainable void ratio range e_{max}-e_{min} leads to the estimate of the maximum change in relative density ΔD_T at $i\rightarrow\infty$ versus initial relative density D_o at $i=0$ during repetitive loading (Chong and Santamarina 2016, Park and Santamarina 2019)

$$\Delta D_T = \frac{e_o - e_T}{e_{max} - e_{min}} \tag{6}$$

$$D_o = \frac{e_{max} - e_o}{e_{max} - e_{min}} \tag{7}$$

Fig. 11 shows the maximum change in relative density anticipated from terminal void ratio e_T versus initial relative density D_o.

The following curve fitting model satisfies the data and allows us to predict the maximum change in relative density ΔD_T as a function of the stress amplitude $\Delta\sigma$ and the initial relative density D_o

$$\Delta D_T = \frac{\Delta\sigma \cdot [1 - D_o]^n}{B} \tag{8}$$

The n-exponent determines the curvature of the model; we use the model exponent $n = 0.7$ in all cases to limit the number of degrees of freedom for curve fitting. The fitted B-parameter tends to increase as the final effective stress σ_f increases. A trend between fitted B-values and the maximum stress σ_f exhibits little data spread due to the emergent tipping points and underlying differences in grain degradation with σ_f. The settlement caused by repetitive loads is the depth integral of vertical strain $\varepsilon_z = (e_o - e_T)/(1+e_o) = \Delta D_T \cdot (e_{max} - e_{min})/(1+e_o)$. Then, the anticipated maximum change in relative density ΔD_T can be used to obtain first order estimates of the maximum settlement a geosystem may experience during repetitive loading.

3.2 Numerical model

The engineering design for the repetitive loading requires advanced constitutive models and explicit numerical scheme. One example from the elastoplastic

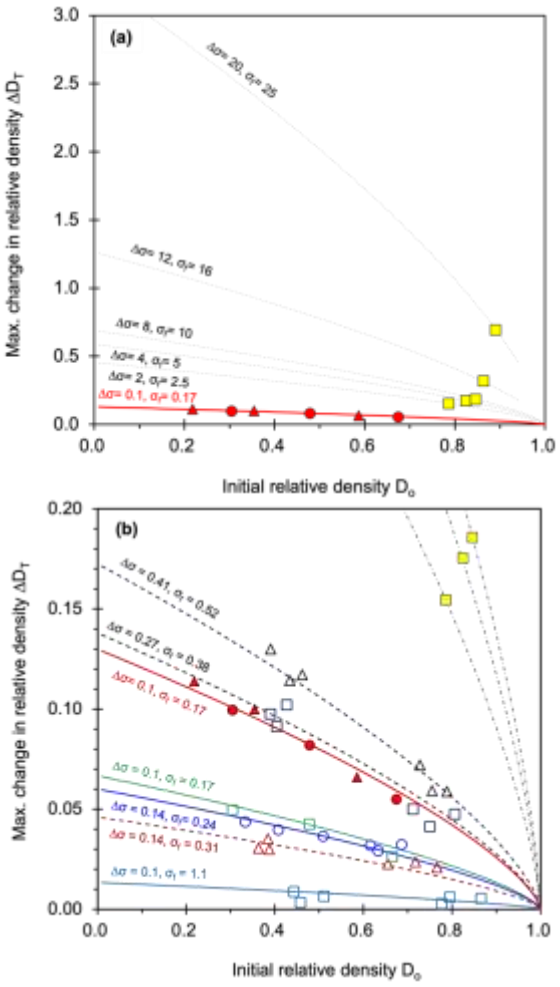

Fig. 11 Maximum change in relative density ΔD_T for both 10^2 high-stress and 10^6 low-stress cycles versus initial relative density D_o at $i=0$ (KAUST 20/30 and Ottawa 20/30 sands). Lines correspond to the fitted Equation 4. Maximum change in relative density (a) full scale $0\leq\Delta D_T\leq 3$ for all tests conducted as part of this study. (b) narrower scale $0\leq\Delta D_T\leq 0.2$ for low-stress (this study) and intermediate stress levels (Modified after Chong and Santamarina 2016 and Park and Santamarina 2019)

framework is bounding surface plasticity which emulates the plastic modulus as a function of the distance between the current stress state and the image point on the bounding surface (Fig. 12 modified from Yu 2007).

The recent development of elasto-plasticity based models involves multi surfaces and kinematic hardening (e.g., memory surface) to simulate the shakedown or ratcheting behavior (Liu *et al*. 2019). Other constitutive functions built on hypoplasticity capture the evolution of soil stiffness with the "incremental nonlinearity" concept (Dafalias 1986, Salciarini and Tamagnini 2009). The early implementation of the incremental nonlinearity concept uses Prandtl-Eryring viscosity constants which capture the logarithmic dependence of the stress on the strain rate (Kolymbas 1991). However, these constitutive models require sophisticated calibration procedures and high

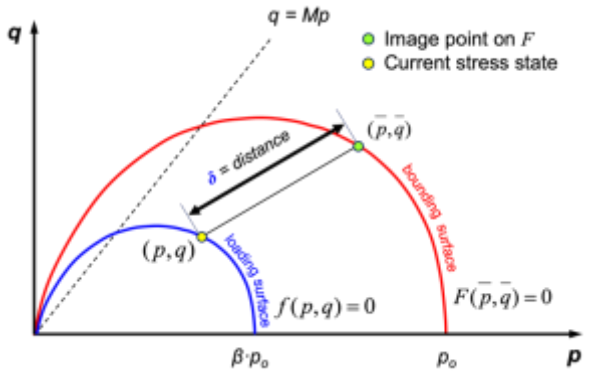

Fig. 12 Bounding surface and loading surface. The yellow circle denotes the current stress state (p, q) on loading surface f and the green circle indicates the image point on bounding surface F. The β-value indicates that the distance δ=0 as $\beta\rightarrow1$ while $\delta=\delta_{max}$ when $\beta\rightarrow0$ (modified after Yu 2007)

computational resources. Moreover, the accumulation of numerical errors in all cases is inevitable with a simulation of a large number of cycles (Niemunis *et al*. 2004). Consequently, the numerical implementation (e.g., FEM, FVM, and MPM) is a challenge for any constitutive models.

The empirical strain accumulation models predict the long-term deformation as a function of load cycles. Overall, there are three groups of accumulation models:

(1) Models describe one component of the accumulated strain (Monismith *et al*. 1975, Lentz and Baladi 1981, Diyaljee and Raymond 1982).
(2) Models predict one component of the accumulated strain at a reference number of cycles (Lentz and Baladi 1980).
(3) Models capture complete strain accumulation as a function of the number of cycles (Suiker and de Borst 2003, Niemunis *et al*. 2005, Chong and Santamarina 2016, Park and Santamarina 2018, Park and Santamarina 2020).

These strain accumulation models have a high numerical stability, but the standalone usage is limited due to the absence of equilibrium and compatibility. Previous constitutive models adopt normality to capture the load-deformation behavior of soils. The concept is robust and well captures the soil response to monotonic loading. However, this study explicitly reveals that the normality may not be valid for soil behavior in response to repetitive loading. Assuming associate flow rule and modified Cam Clay yield surface, plastic strain is not normal to the monotonic plastic potential anymore in view of asymptotic conditions as i $\rightarrow\infty$; plastic volumetric strain approaches to zero (i.e., terminal void ratio) while shear strain still occurs in either shakedown or ratcheting mode.

Alternatively, the hybrid solutions from formal to sui-generis combine the constitutive model (e.g., modified Cam clay model) and empirical strain accumulation model to overcome their shortcomings. The hybrid constitutive model considers the monotonic preloading and the first load cycle; then the empirical strain accumulation model fits the strain evolutions and asymptotic shear and volumetric trends during the load cycles. This methodology can be extended to other kinds of repetitive loading, including heating and cooling, freeze-thaw cycles, wet-dry cycles, and fluid pressure cycles (Kakroudi *et al*. 2024, Zhao *et al*. 2024, Ibdah *et al*. 2025).

4. Conclusions

This study investigates the long-term behavior of granular materials and geosystems subjected to repetitive mechanical loads. The repetitive load-induced stress paths depend on the type of geo-structure, loading direction, periodicity, and boundary conditions. Enhanced understanding of long-term performance of geosystems subjected to repetitive loads is critical for designing sustainable energy geo-structures. The findings of this study provide a foundation for further development of test protocols, models, and algorithms for assessing the performance and safety of these systems. Conclusions made in this study follows:

- Repetitive loading leads to granular degradation, influencing the mechanical properties of materials, such as shear strength, compressibility, and hydraulic conductivity. The degradation mechanisms vary with stress levels and the number of cycles, with particle crushing dominating at high-stress cycles and surface abrasion prevailing under low-stress conditions.
- The presence of fines significantly impacts the long-term performance of sand-fines mixtures. A threshold fines fraction influences the volumetric response with fines either separating coarse grains or occupying voids. In fact, fines behavior leads to different deformation response as the number of loading cycles increases.
- Small-strain stiffness measurements and resilient modulus data are crucial for understanding the stiffness evolution of sediments under repetitive loading. The relationship between resilient modulus and shear modulus can provide insights into deformation behaviors with significant changes in stiffness.
- A new dimensionless shear stress ratio $\tau^*=(\tau_o+\Delta\tau)/\tau ult$ successfully predicts transitions between shakedown and ratcheting modes, accounting for initial stress state, loading amplitude, and material strength characteristics.
- The hybrid numerical modeling strategy combines rigorous constitutive models with computationally efficient empirical strain accumulation formulations, addressing computational challenges in high-cycle simulations while maintaining engineering accuracy.

Acknowledgments

This work was supported by Post-Doctor LAB employment support Program (INU SURE LAB Program) (2024) in the Incheon National University.

References

Al-Qadi, I.L., Wang, H. and Tutumluer, E. (2010), "Dynamic analysis of thin asphalt pavements by using cross-anisotropic stress-dependent properties for granular layer", *Transport. Res. Record*, **2154**(1), 156-163. https://doi.org/10.3141/2154-16.

Brown, S.F. (1996), "Soil mechanics in pavement engineering", *Géotechnique*, **46**(3), 383-426. https://doi.org/10.1680/geot.1996.46.3.383.

Cha, M., Santamarina, J.C., Kim, H.S. and Cho, G.C. (2014), "Small-strain stiffness, shear-wave velocity, and soil compressibility", *J. Geotech. Geoenviron. Eng.*, **140**(10), 06014011. https://doi.org/10.1061/(ASCE)GT.1943-5606.0001157.

Cha, W., Park, J. and Santamarina, J.C. (2023), "Long-term response of sand subjected to repetitive simple shear loading: Shakedown, ratcheting, and terminal void ratio", *J. Geotech. Geoenviron. Eng.*, **149**(6), 04023028. https://doi.org/10.1061/JGGEFK.GTENG-10814.

Dafalias, Y.F. (1986), "Bounding surface plasticity. I: Mathematical foundation and hypoplasticity", *J. Eng. Mech.*, **112**(9), 966-987. https://doi.org/10.1061/(ASCE)0733-9399(1986)112:9(966).

Daramola, O. (1980), "Effect of consolidation age on stiffness of sand", *Geotechnique*, **30**(2), 213-216. https://doi.org/10.1680/geot.1980.30.2.213.

Diyaljee, V.A. and Raymond, G.P. (1982), "Repetitive load deformation of cohesionless soil", *J. Geotech. Eng. Division*, **108**(10), 1215-1229. https://doi.org/10.1061/AJGEB6.0001348.

Drnevich, V.P. and Richart Jr, F.E. (1970), "Dynamic prestraining of dry sand", *J. Soil Mech. Found. Division*, **96**(2), 453-469. https://doi.org/10.1061/JSFEAQ.0001398.

Fleming, P.R., Frost, M.W. and Lambert, J.P. (2007), "Review of lightweight deflectometer for routine in situ assessment of pavement material stiffness", *Transport. Res. Record*, **2004**(1), 80-87. https://doi.org/10.3141/2004-09.

FHWA (1996), Resilient modulus of unbound granular base/ subbase materials and subgrade soils long-term pavement performance protocol 46. Federal Highway Administration Pavement Performance Division.

Feda, J. (2002), "Notes on the effect of grain crushing on the granular soil behaviour", *Eng. Geol.*, **63**(1-2), 93-98. https://doi.org/10.1016/S0013-7952(01)00072-2.

Fleming, P.R., Frost, M.W. and Lambert, J.P. (2007), "Review of lightweight deflectometer for routine in situ assessment of pavement material stiffness", *Transport. Res. Record: J. Transport. Res. Board*, **2004**(1), 80-87. https://doi.org/10.3141/2004-09.

Hafez, A., Liu, Q., Finkbeiner, T., Alouhali, R.A., Moellendick, T. E. and Santamarina, J.C. (2021), "The effect of particle shape on discharge and clogging", *Scientific Reports*, **11**(1), 3309. https://doi.org/10.1038/s41598-021-82744-w.

Hicks, R.G. and Monismith, C.L. (1971), "Factors influencing the resilient response of granular materials", *Highway Res. Record*, (345), 15-31.

Ibdah, L., Owusu, K., Behdad, A. and Eun, J. (2025), "Effects of freeze-thaw cycles on the unconfined compressive strength of lime-and cement-stabilized soils", *Geomech. Eng.*, **41**(1), 59-70. https://doi.org/10.12989/gae.2025.41.1.059.

Indraratna, B. and Redana, I.W. (1997), "Plane-strain modeling of smear effects associated with vertical drains", *J. Geotech. Geoenviron. Eng.*, **123**(5), 474-478. https://doi.org/10.1061/(ASCE)1090-0241(1997)123:5(474).

Kakroudi, H.A., Bayat, M. and Nadi, B. (2024), "Static and dynamic characteristics of silty sand treated with nano-silica and basalt fiber subjected to freeze-thaw cycles", *Geomech. Eng.*, **37**(1), 85-95. https://doi.org/10.12989/gae.2024.37.1.085.

Kim, I.T. and Tutumluer, E. (2005), "Unbound aggregate rutting models for stress rotations and effects of moving wheel loads", *Transport. Res. Record*, **1913**(1), 41-49. https://doi.org/10.1177/0361198105191300105.

Kim, S.Y., Park, J., Cha, W., Lee, J.S and Carlos Santamarina, J. (2021), "Soil response during globally drained and undrained freeze–thaw cycles under deviatoric loading", *J. Geotech. Geoenviron. Eng.*, **147**(2), 06020030. https://doi.org/10.1061/(ASCE)GT.1943-5606.0002464.

Kolymbas, D.I.H.D. (1991), "An outline of hypoplasticity", *Arch. Appl. Mech.*, **61**(3), 143-151. https://doi.org/10.1007/BF00788048.

Lackenby, J., Indraratna, B., McDowell, G. and Christie, D. (2007), "Effect of confining pressure on ballast degradation and deformation under cyclic triaxial loading", *Géotechnique*, **57**(6), 527-536. https://doi.org/10.1680/geot.2007.57.6.527.

Lekarp, F. and Dawson, A. (1998), "Modelling permanent deformation behaviour of unbound granular materials", *Constr. Build. Mater.*, **12**(1), 9-18. https://doi.org/10.1016/S0950-0618(97)00078-0.

Lentz, R.W. and Baladi, G.Y. (1980), "Prediction of permanent strain in sand subjected to cyclic loading", *Transport. Res. Record*, (749).

Lentz, R.W. and Baladi, G.Y. (1981), "Constitutive equation for permanent strain of sand subjected to cyclic loading", *Transport. Res. Record*, **810**, 50-54.

Liu, H.Y., Abell, J.A., Diambra, A. and Pisanò, F. (2019), "Modelling the cyclic ratcheting of sands through memory-enhanced bounding surface plasticity", *Géotechnique*, **69**(9), 783-800. https://doi.org/10.1680/jgeot.17.P.307.

Mayne, P.W. and Kulhawy, F.H. (1982), "Ko-OCR relationships in soil", *J. Geotech. Eng. Division*, **108**(6), 851-872. https://doi.org/10.1061/AJGEB6.0001306.

Monismith, C.L., Ogawa, N. and Freeme, C.R. (1975), "Permanent deformation characteristics of subgrade soils due to repeated loading", *Transport. Res. Rrecord*, (537).

Niemunis, A., Wichtmann, T. and Triantafyllidis, T. (2004), "Explicit accumulation model for cyclic loading", Proc., Int. Conf. on Cyclic Behaviour of Soils and Liquefaction Phenomena, Taylor & Francis, London, 65-76.

Niemunis, A., Wichtmann, T. and Triantafyllidis, T. (2005), "A high-cycle accumulation model for sand", *Comput. Geotech.*, **32**(4), 245-263. https://doi.org/10.1016/j.compgeo.2005.03.002.

NCHRP (2004), Laboratory determination of resilient modulus for flexible pavement design National Cooperative Highway Research Program NCHRP Project 1-28A. Transportation Research Board of the National Academies.

Papadopoulos, E., Cortes, D.D. and Carlos Santamarina, J. (2016), "In-situ assessment of the stress-dependent stiffness of unbound aggregate bases: application in inverted base pavements", *Int. J. Pavement Eng.*, **17**(10), 870-877. https://doi.org/10.1080/10298436.2015.1022779.

Papadopoulos, E. and Santamarina, J.C. (2016), "Analysis of inverted base pavements with thin-asphalt layers", *Int. J. Pavement Eng.*, **17**(7), 590-601. https://doi.org/10.1080/10298436.2015.1007232.

Pasten, C. and Carlos Santamarina, J. (2011), "Energy geo-storage—analysis and geomechanical implications", *KSCE J. Civil Eng.*, **15**(4), 655-667. https://doi.org/10.1007/s12205-011-0006-6.

Park, J. and Santamarina, J.C. (2017), "Revised soil classification system for coarse-fine mixtures", *J. Geotech. Geoenviron. Eng.*, **143**(8), 04017039. https://doi.org/10.1061/(ASCE)GT.1943-5606.0001705.

Qiu, J., Xie, Y., Chen, Y., Reissenweber, B., Wang, C., Wang, Z., and Xue, J. (2025), "Investigating rutting performance of unpaved roads with recycled concrete aggregates using small-

scale cyclic loading tests", *Geomech. Eng*., **41**(2), 221-232. https://doi.org/10.12989/gae.2025.41.2.221.
Park, J. and Santamarina, J.C. (2019), "Sand response to a large number of loading cycles under zero-lateral strain conditions: Evolution of void ratio and small strain stiffness", *Géotechnique*, **69**(6), 501-513. https://doi.org/10.1680/jgeot.17.P.124.
Park, J. and Santamarina, J.C. (2020), "Soil response to repetitive changes in pore water pressure under deviatoric loading.", *J. Geotech. Geoenviron. Eng*., **146**(5), 04020023. https://doi.org/10.1061/(ASCE)GT.1943-5606.0002229.
Park, J. and Santamarina, J.C. (2023), "Sands subjected to repetitive loading cycles and associated granular degradation", *Geotech. Geoenviron. Eng*., **149**(11). https://doi.org/10.1061/JGGEFK.GTENG-11153.
Salciarini, D. and Tamagnini, C. (2009), "A hypoplastic macroelement model for shallow foundations under monotonic and cyclic loads", *Acta Geotech.*, **4**(3), 163-176. https://doi.org/10.1007/s11440-009-0087-2.
Sadrekarimi, A. and Olson, S.M. (2010), "Particle damage observed in ring shear tests on sands", *Can. Geotech. J*., **47**(5), 497-515. https://doi.org/10.1139/T09-117.
Santamarina, J.C., Klein, K.A. and Fam, M.A. (2001), Soils and waves (Vol. 316). New York: J. Wiley & Sons.
Sawicki, A. and Swidzinski, W. (1995), "Cyclic compaction of soils, grains and powders", *Powder Technol*., **85**(2), 97-104. https://doi.org/10.1016/0032-5910(95)03013-Y.
Schuettpelz, C.C., Fratta, D. and Edil, T.B. (2010), "Mechanistic corrections for determining the resilient modulus of base course materials based on elastic wave measurements", *J. Geotech. Geoenviron. Eng*., **136**(8), 1086-1094. https://doi.org/10.1061/(ASCE)GT.1943-5606.0000329.
Suiker, A.S.J. and de Borst, R. (2003), "A numerical model for the cyclic deterioration of railway tracks", *Int. J. Numer. Method. Eng.*, **57**(4), 441-470. https://doi.org/10.1002/nme.683.
Tutumluer, E. and Seyhan, U. (1999), "Laboratory determination of anisotropic aggregate resilient moduli using an innovative test device", *Transport. Res. Record*, **1687**(1), 13-21. https://doi.org/10.3141/1687-0.
Werkmeister, S., Dawson, A.R. and Wellner, F. (2005), "Permanent deformation behaviour of granular materials", *Road. Mater. Pavement*, **6**(1), 31-51. https://doi.org/10.1080/14680629.2005.9689998.
Williams, R.R. and Nazarian, S. (2007), "Correlation of resilient and seismic modulus test results", *J. Mater. Civil Eng*., **19**(12), 1026-1032. https://doi.org/10.1061/(ASCE)0899-1561(2007)19:12(1026).
Wichtmann, T., Niemunis, A. and Triantafyllidis, T. (2005), "Strain accumulation in sand due to cyclic loading: drained triaxial tests", *Soil. Dyn. Earthq. Eng.*, 25(12), 967-979. https://doi.org/10.1016/j.soildyn.2005.02.022.
Wichtmann, T., Niemunis, A. and Triantafyllidis, T. (2010), "Strain accumulation in sand due to drained cyclic loading: on the effect of monotonic and cyclic preloading (Miner's rule)", *Soil Dyn. Earthq. Eng*., **30**(8), 736-745. https://doi.org/10.1016/j.soildyn.2010.03.004.
Wu, T., Cai, Y., Guo, L., Ling, D. and Wang, J. (2017), "Influence of shear stress level on cyclic deformation behaviour of intact Wenzhou soft clay under traffic loading", *Eng. Geol.*, **228**, 61-70. https://doi.org/10.1016/j.enggeo.2017.06.013.
Yu, H.S. (2007), Plasticity and geotechnics, Springer, N.
Zhao, J., Yang, P., Li, L., Zhang, T. and Wang, H. (2024), "Influence of freeze thaw on stress-strain characteristics and microstructure of cement and fly ash stabilized organic soil", *Geomech. Eng*., **39**(6), 529-546. https://doi.org/10.12989/gae.2024.39.6.529.

IC